

FTIR analysis determines the spectrum of infrared wavelengths that a substance absorbs. The schematic for the FTIR is shown in Figure 6. To do this, samples of the material are exposed to infrared radiation (IR). To ascertain the material's molecular makeup and structure, the sample's capacity to absorb energy from infrared light at various wavelengths is measured. An extensive database of reference spectra is searched against the IR spectrum to identify unknown materials. As long as it is possible to create a standard curve of known concentrations of the component of interest, materials can be quantified using the FTIR materials characterization technique. Unknown materials, additives found in polymers, surface contamination on a material, and more can all be found using FTIR analysis. The results of the tests can identify the molecular structure and composition of a sample. To identify samples, a straightforward tool called an interferometer creates an optical signal that has all the IR frequencies encoded into it. It is quick to measure the signal. The signal is then decoded using a mathematical process called the Fourier transformation. The spectral data is then mapped using this computer-generated process. The spectrum that results from this graph is then identified by searching it against reference libraries.

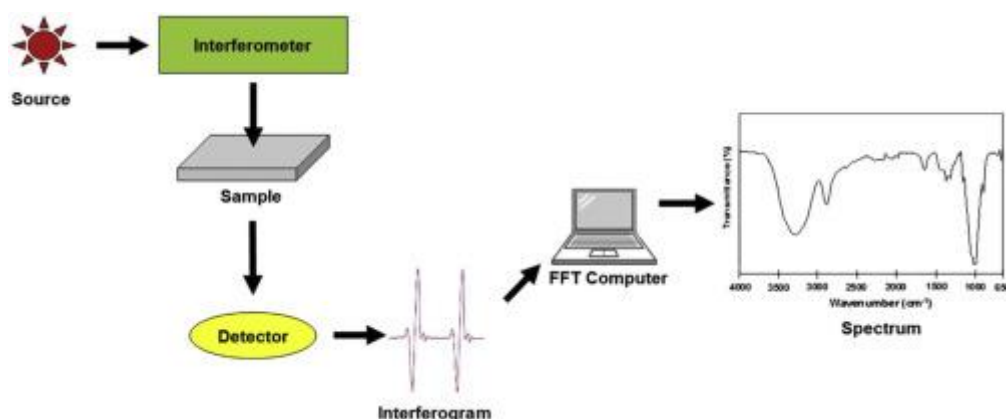


Figure 6: FTIR spectroscopy principle (Mathias, 2022).

3.3.3 HR-TEM

The morphology and the particle size distribution of *Cotyledon*-AgNPs were determined by HR-TEM analysis using a FEI Tecnai G2 F20 field-emission. TEM samples were prepared by drop-casting the AgNPs on carbon-coated grids and allowed to dry at room temperature, prior to measurement. The same samples were also examined using HR-TEM for Selected Area Electron Diffraction (SAED) and Energy-dispersive X-ray spectroscopy (EDX) studies. Software called Image J was used to determine the particle size distribution.

Electrons are made to pass through the specimen, and the image is formed on the fluorescent screen using either the transmitted or diffracted beam. It is made up of an electron gun that generates electrons. A magnetic condensing lens is used to condense the electrons and to control the size of the electrons that fall onto the specimen. As shown in Figure 7, the specimen is placed between the condensing and objective lenses. The magnetic objective lens is used to block the high-angle diffracted beam, and the aperture is used to eliminate any diffracted beam, increasing image contrast. To achieve higher magnification, the magnetic projector lens is placed above the fluorescent screen. A fluorescent screen or a camera can be used to capture the image (CCD – Charged Coupled device). The morphology and the particle size distribution of *Cotyledon*-AgNPs were determined by HR-TEM analysis using an FEI Tecnai G2 F20 field emission.

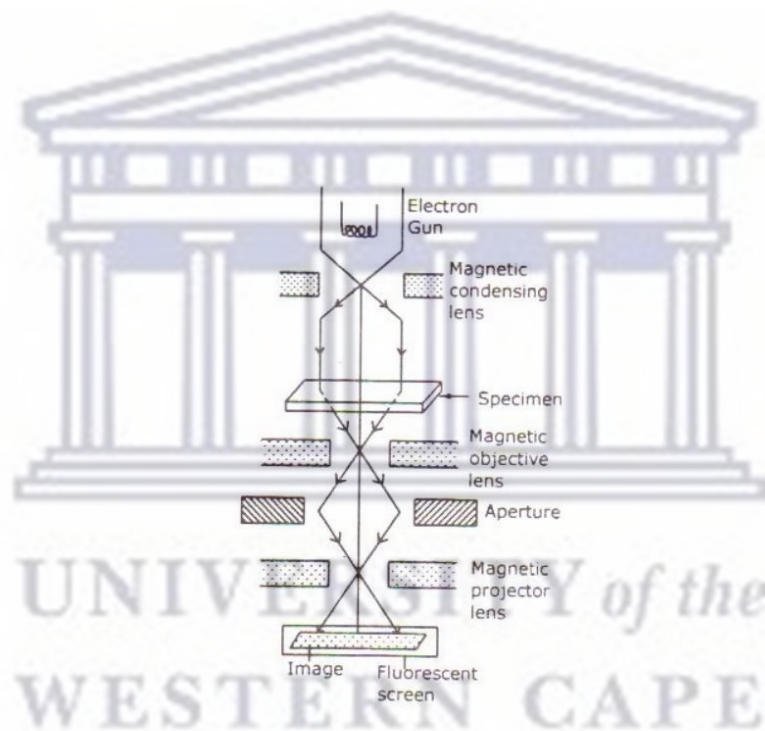


Figure 7: HRTEM working principle (BrainKart, 2018).

3.3.4 DLS

The particle size, the size distribution, zeta-potential, and the peak intensity of the AgNPs was determined by DLS using Zetasizer nano series Nano ZS, Malvern Instrument, UK. The DLS measurements were carried-out for size ranges from 0.1 to 100 nm.

Dynamic Light Scattering (DLS) is a popular light scattering technique because it allows for particle sizes as small as 1 nm in diameter. Emulsions, micelles, polymers, proteins, nanoparticles, and colloids are common applications. A laser beam illuminates the sample, and the fluctuations of the scattered light are detected by a fast photon detector at a known scattering

angle. Simple DLS instruments with a fixed angle of measurement can determine the mean particle size in a limited size range. Multi-angle instruments with greater sophistication can determine the entire particle size distribution. From a microscopic perspective, the particles scatter light, imprinting information about their motion. As shown in Figure 8, analysing the fluctuation of the scattered light yields information about the particles. The particle size, size distribution, zeta-potential, and peak intensity of the AgNPs were determined by DLS using Zetasizer nano series Nano ZS, Malvern Instrument, UK. The DLS measurements were carried out for size ranges from 0.1 to 100 nm.

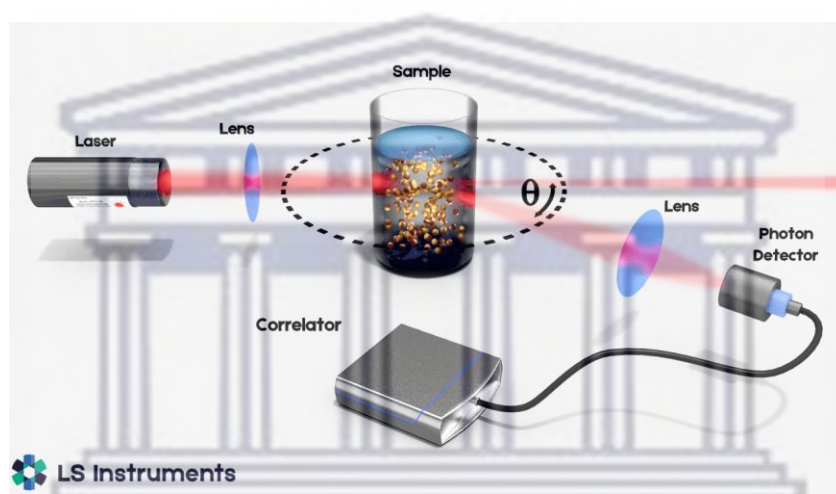


Figure 8: DLS working principle (LS Instruments, 2022).

3.4 Biological activity of the AgNPs

The biological activity of the AgNPs was assessed in agreement with biosafety level 2 guidelines at the Biolabels Node research labs (Department of Biotechnology, UWC). The laboratory disposed of the biological waste in accordance with the disposal technique outlined in their normal operating procedures. All the bacterial strains were obtained from ATCC (Manassas, USA).

3.4.1 Stability testing of SBH-AgNPs

The stability of the *Cotyledon*-AgNPs was evaluated in different biological media and buffers used in this study were Mueller Hinton broth (MHB) and LB broth. MHB and LB are used for determining minimal inhibitory concentrations (MICs), commonly used for antibiotic

susceptibility testing, specifically disk diffusion tests. In glass test tubes, 250 μL of aqueous solutions of *SBH*-AgNPs were mixed with the same volume of the medium or buffer. The tubes were incubated at 25 °C or 37 °C for 24 h. The stability of these nanoparticles was evaluated by measuring changes in their Ultraviolet-Visible spectroscopy (UV-Vis) spectra.

3.4.2 Antibacterial activity of AgNPs

The agar well diffusion method was used as described by (Boorn et al., 2010a) where the antibacterial activity of the synthesized AgNPs was evaluated on six bacterial strains of *S. aureus*, *S. epidermidis*, MRSA, *K. pneumoniae*, *E. coli* and *P. aeruginosa*.

Microbial suspensions of the bacteria were cultured in MHB broth and diluted until they reached a 0.5 McFarland standard (standard is approximately 1×10^8 CFU/mL). A volume of 50 μL of the microbial suspensions was added to each well containing MHB and AgNPs of 63 $\mu\text{g}/\text{mL}$ concentration. The plates were sealed and incubated for 24 h at 37 °C and the zone of inhibitions were observed and determined. Ciprofloxacin (2 $\mu\text{g}/\text{mL}$) was used as positive control for the bacteria, while sterile deionized water was used as the negative control. An inhibition zone with diameter greater than 10 mm is considered as positive antagonism effect.

3.4.3 Determination of minimum inhibition concentration

The microbial suspensions were applied in volumes of 50 μL to each well containing MHB broth and AgNPs. The plates were sealed and kept at 37 °C for 24 hours. The negative control was sterile deionized water, while the positive control for the microorganisms was ciprofloxacin (2 $\mu\text{g}/\text{mL}$).

After the initial incubation, in each well 10 μL of Alamar Blue was added, and the plate underwent a further three hours of dark incubation. The non-fluorescent Alamar Blue dye (resazurin) was transformed into the extremely fluorescent pink chemical resofurin in the presence of live bacteria. A spectrophotometer was then used to determine the MIC at a wavelength of 530-560/590 nm for fluorescence excitation and emission. Three duplicates of the screening were conducted. The MIC was reported as the lowest Ag-NP concentration that inhibited bacterial growth and MBC as the Ag-NP concentration that showed no bacterial growth.

Chapter 4

Results and discussion

4.1 Synthesis of SBH-reduced AgNPs

The synthesis of AgNPs using honey is suggested to be plausible due to the presence of phenolic substances and sugars present in the honey which reduces the Ag^+ ions into metallic silver (Haiza, et al., 2013). In a study by Haiza and colleagues, they reported the green synthesis of silver nanoparticles using honey as the reducing agent. They suggested that the sucrose, glucose and even proteins and enzymes play a role in the reduction process. The synthesised AgNPs exhibited dark brown colour (See Figure 9) due to an excitation of the surface plasmon vibrations of the ionic AgNPs and the reduction of silver ions by phenolics and sugars to form metallic AgNPs (Hasim et al., 2020), (Khorrami et al., 2019).



Figure 9: Visual representation of the synthesis of silver nanoparticles, indicated by the colour change of the solution from colourless to brown.

According to an earlier research, honey has a significant amount of phenolic chemicals, reducing sugars, proteins, and vitamins as organic and natural molecules. The reduction of silver nitrate, as suggested above, may involve phenolic and reducing substances like fructose and glucose (Khorrami et al., 2019). The schematic depicting how honey's bioactive ingredients help reduce silver ions to silver nanoparticles is shown in Figure 4. In a different study by Khorrami and colleagues they also synthesized AgNPs using honey and observed a colour change from light yellow to brown in the solution containing honey and silver nitrate.

Similarly, they reported that the compounds responsible for the silver nitrate reduction process were fructose, sucrose and the phenolic compounds. These studies support the fact that honey through its constituents is responsible for the reduction of silver ions to silver atoms. Additionally, the colour change observed in the reported literature is similar to the one obtained in this study.

4.2 Optimization of synthesis

In every synthesis protocol, it is essential that the parameters necessary for generating a desired product need to be optimized for better results. An optimization is carried out to determine the optimal experimental conditions for a reaction synthesis. The AgNO₃ concentration, reaction time, pH, and the involvement of reducing agents in promoting a reaction are some of the variables that affect the formation of Ag-NPs. Therefore, the direct control of these parameters is a critical factor that affects the biosynthesis and characteristics of the nanoparticles. In the literature, Ghafari et al., (2014) reported the synthesis of silver nanoparticles using a plant extract. When the synthesis was carried out in various reaction conditions such as the extract concentrations, pH and mixing ratio of the reactants were investigated (Ghafari-Moghaddam & Hadi-Dabanlou, 2014).

An UV-visible spectrophotometer was employed for the spectrometric analysis of honey synthesized silver nanoparticles. Free electrons in the silver nanoparticles evoked by absorbing visible light and transmitted to a higher energy level is unstable at the excited state, therefore has to return to the base energy level simultaneously emitting a photon (Behravan et al., 2019). This phenomenon gives rise to the surface plasmon resonance (SPR) peak commonly known as the absorption band. Many previous literature reports indicate that the absorption band of AgNPs are visible at around 400-490 nm in the UV-visible spectra. According to a study by Gonzalez and colleagues, an ecologically friendly method for generating silver nanoparticles in water under ambient conditions using natural honey was reported. The obtained silver nanoparticles were characterised by using UV-vis spectroscopy giving the SPR band at around 413 nm (Gonzalez, et al., 2017). The SPR peaks and line widths are descriptive of the size and shape of the nanoparticles and their height provides information on the concentration of AgNPs since the maximum SPR is directly proportional to the concentration of AgNPs. The UV-vis absorption peak is widely known for providing information on the degree of dispersion of silver nanoparticles. The greater the degree of dispersion of nanoparticles, the narrower the absorption peak (Philip, 2010). We shall now look at the pH as one of the important parameters.

4.2.1 Effect of pH

A pH of a solution is a measure of how basic or acidic a solution is. The pH scale ranges from 0 to 14. A pH value of 7 is considered neutral on this scale, meaning it is neither acidic nor basic. It is more acidic if the pH value is below 7, and more basic if the pH value is above 7 (Yuqing, et al., 2005). Previous studies have pointed out that, reduction of Ag^+ to Ag is assisted by a high pH which was always achieved by the addition of NaOH. The alkaline environment facilitates the opening of the glucose ring by the abstraction of the α -proton of the ring oxygen and subsequently glucose is oxidized to gluconic acid (Siddiqui et al., 2018), (Philip, 2010). The effect of pH on the synthesis of honey reduced AgNPs was evaluated, and Figure 10 shows the different absorption bands obtained from using different pHs values. As depicted in figure 10 at lower pH, the SPR band is not visible but at pH 9 and 10 the SPR characteristic of AgNPs is present which suggests that nanoparticles are formed at higher pH values. Thus, it can be concluded that the effect of pH plays a vital role in AgNPs formation for green synthesis of SBH reduced nanoparticles. According to previous studies it was found that nanoparticles form at higher pH values which explains why there are no observed SPR peaks of AgNPs at acidic pH values.

In a study done by Hosny and colleagues, they synthesized AgNPs using honey at different pH and were able to successfully obtain the nanoparticles at an alkaline pH= 10 (Hosny et al., 2017). Another study by Philip, (2010) investigated the preparation of silver nanoparticles using honey. In their findings, they observed that the SPR peak was smoother and narrower as the pH was increasing. The desired uniformly distributed peak was observed at pH of 8.5 whereas, at lower pH values the absorbance peak was broader and less intense (Philip, 2010). In a different study, Youssef et al, 2019 reported an eco-friendly synthesis of AgNPs from an Egyptian honey. They evaluated the effect of pH on the formation of the nanoparticles at pH values of 5, 6, 7, 8 and 9. In their findings, a sharp peak with the maxima absorbance was observed at the pH value of 9 (Youssef et al., 2019).

Therefore, it can be concluded that the best pH for synthesizing these nanoparticles under these conditions is generally at pH 10. Contrastingly, another study by (González Fa et al., 2017) synthesized AgNPs using honey at pH values of 5 and 10. They both gave surface plasmon resonance bands at about 400 nm. However, the former pH was used under an increased honey concentration, the plasmon spectral band changed to a shorter wavelength, indicating a reduction in particle size. This observation does suggest that in some instances the reduction

of silver ions may take place at pH values lower than 7. The explanation behind this observation indicated that there is a possibility of the reactive fructose component taking part in the reduction reaction alongside the glucose, and vitamin C which are all reducing agents found in honey. The addition of the alkaline NaOH serves to induce the Ag ions reduction. The metal ions oxidize glucose to gluconic acid, while the base aids the opening of the glucose ring by abstracting the α -proton of the sugar ring oxygen (Philip, 2010). According to (Philip, 2010) as the pH is increased, the SPR band gets sharpened.

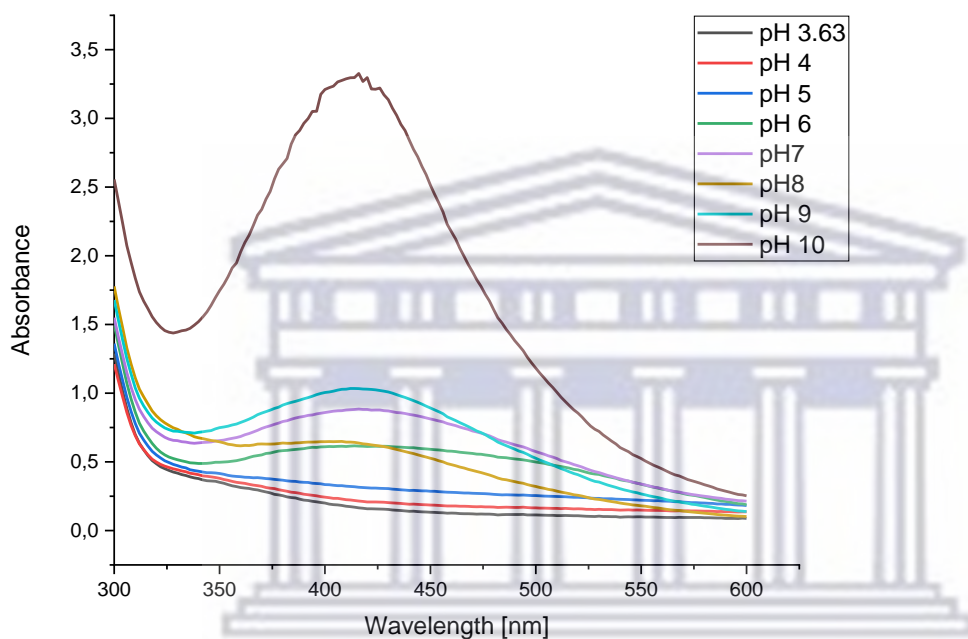


Figure 10: UV-Vis absorbance spectra of AgNPs at 100 °C and 50mg/mL Honey concentration at different pH values.

4.2.2 Effect of temperature

It has been long established that when the reaction temperature rises, the reaction rate and particle production rate increase in a reaction. Due to this fact, the temperature in which a reaction occurs plays a huge role on the production of nanoparticles (Shah et al., 2015). To investigate the effect of temperature, the reaction mixture of SBH and AgNO₃ were allowed to react at different heating temperatures of 25°C, 50°C, 75°C and 100°C. The selected temperatures for the study were comparable previously reported by other researchers in the literature. For example, for a start, Haiza et al, 2013 successfully synthesized silver nanoparticles using honey at room temperature (Haiza, et al., 2013). In a different study, the synthesis of AgNPs was carried out 70 °C (Czernel et al., 2021). The samples were removed from the thermo-shaker and the UV-vis spectra analysed. Figure 11 shows that, the changes in

the intensity of the SPR band are strongly affected by the synthesis temperature. It is hypothesized that high temperatures will enable faster production of nanostructures due to Ostwald's ripening. Additionally, it has been discovered that the temperature at which nanoparticles made from plant extracts are synthesized can influence their size, shape, and production (Shah et al., 2015), (Liu et al., 2011). For instance, the synthesis of Ag nanoparticles using *Citrus sinensis* (sweet orange) peel extract at a reaction temperature of 25 °C resulted in particles with an average size of about 35 nm. However, the average particle size dropped to 10 nm when the reaction temperature was raised to 60 °C. According to their findings, at room temperature, the reaction took up to 75 minutes to complete. Contrastingly, at 60 °C, the reaction was completed in 45 minutes saving a whole half an hour period. The rise in temperature was responsible for this observation while smaller nanoparticles eventually form as a result of the reactants being consumed quickly. (Kaviya, et al., 2011). A further support was shown by the SPR peak obtained from the UV-vis spectra of the synthesized AgNPs at 60 °C which gave an intense peak than that of the 25 °C reaction.

At 75°C, the fast formation of AgNPs was observed, with the resonance absorption intensity being increased with the reaction temperature. For lower temperatures of 50 °C and even lower 25 °C, the intensity peak was absent at the region of 400 nm which shows that no AgNPs were formed.

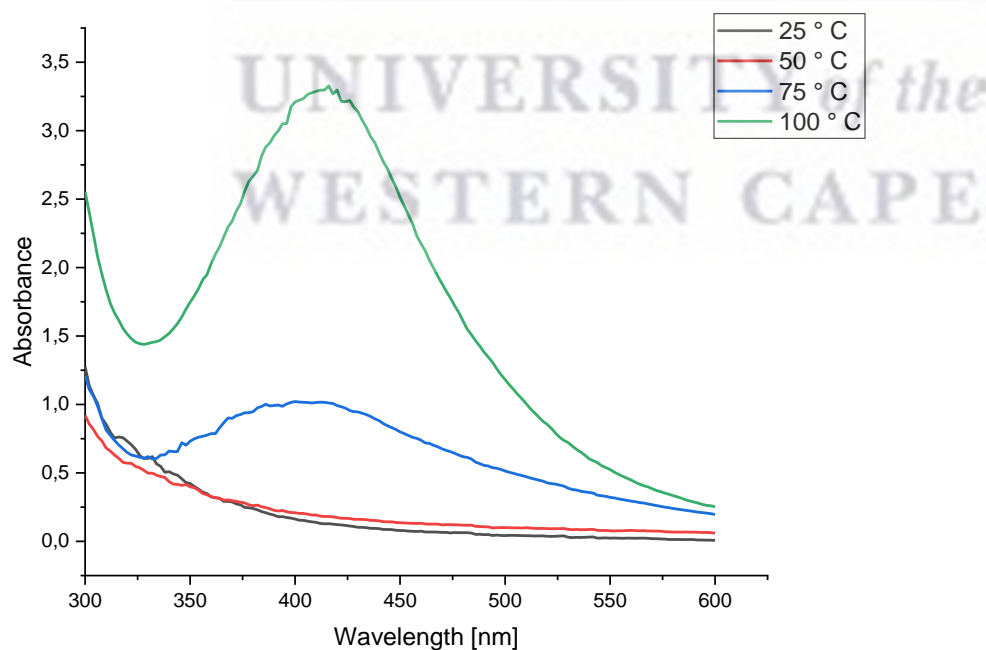


Figure 11: UV-Vis spectra of AgNPs at pH 10 and 50mg/mL Honey concentration under different temperatures.

Comparing the absorbance peak intensity at 100 °C and the one at 75 °C it can be clearly seen that the most favourable conditions for this synthesis are at higher temperatures. The intensity of the SPR peak increases with increasing temperatures which agrees with the study already reported above by Kayiva et al., (2011). Similarly, the immediate previous literature report does support this observation. In a study conducted by Stavinskaya and colleagues, where they synthesized silver nanoparticles by using *Vitex agnus-cactus* extract and investigated the effect of temperature on their synthesis by varying the temperatures from 40-80 °C (Stavinskaya et al., 2019). As expected, they found out that the intensity of the SPR peak increased with increasing temperature. It was observed that at 80 °C, fast formation of AgNPs had occurred indicating a higher SPR peak intensity. Whereas, at lowest study temperatures of 40 °C the SPR band was lower and did not produce a pronounced signal at the region of 400 nm.

Similarly, in another study AgNPs were synthesized using honey while varying the reaction temperatures from 35 °C to 70 °C. The UV-vis results of AgNPs synthesized at the temperature of 70 °C, had a band with the highest intensity (Czernel et al., 2021). Hence it was deduced that when the temperature reaches 70 °C, specific interactions, mainly hydrogen and van der Waals bonds, break, and initiates the monomerization processes. Additionally, a higher temperature significantly speeds up the Ag⁺ ion reduction reaction.

Therefore, it can be concluded that higher temperatures speed up the formation of AgNPs hence there will be more nanoparticles produced at higher temperatures compared to lower temperatures. Conclusively, the temperature range which gave favourable results ranges between 50 °C to 80 °C alongside a supporting pH. Our synthesis is about developing friendly conditions which abide by the green synthesis guidelines, the 100 °C temperature was out of our selection because it was still plausible to obtain AgNPs at lower temperatures of 75 °C hence it was the working temperature of choice.

4.2.3 Effect of SBH concentration

In order for the green synthesis of nanoparticles to take place, Ag⁺ ions require a biological reducing agent. Most of the time, reducing agents also function as coating and stabilizing agents. In this method, nanoparticles are synthesized using stingless bee honey (SBH), which is reported to possess antimicrobial properties, thereby enhancing the effect of the nanoparticles through synergistic effects. The concentration of the reducing agent has an effect on the properties, rate and quantity of nanoparticles produced in a reaction (Behravan et al., 2019).

The effect of SBH concentration on the formation of AgNPS was studied by varying the concentration of the honey solutions as shown in Figure 12.

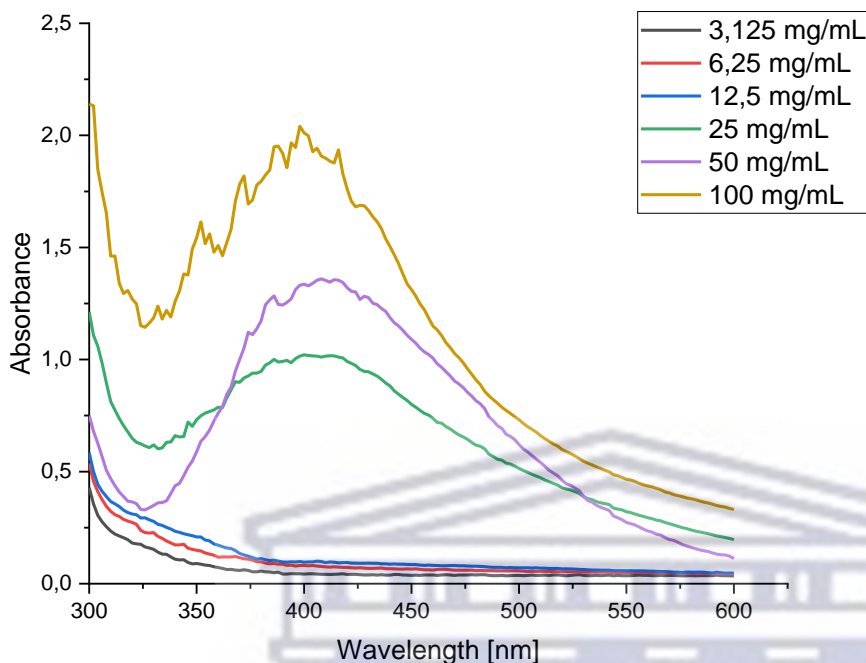


Figure 12: UV-Vis spectra of AgNPs at 75 °C and pH 10 at varying SBH concentrations.

The synthesis at pH 10 at 75 °C temperature was carried out using different SBH concentrations in order to assess the impact of the SBH concentration on the formation of silver nanoparticles. In each instance, surface plasmon resonance bands were identified and recorded.

The UV-vis spectra shown above (Figure 12) is the intensity of SPR peak obtained by changing the concentration of the honey solution while keeping the reaction temperature at 75 °C. The results showed that the higher the concentrations of the SBH the higher the absorbance. It should be noted that with increased honey concentration, the plasmon spectral band changed to a shorter wavelength, indicating a reduction in particle size. Theoretically and experimentally, it is found that when size decreases, the SPR peak shifts towards shorter wavelength side (Haiza, et al., 2013). Haiza et al., (2013) reported the synthesis of silver nanoparticles using honey and studied the effects of different honey concentrations (10g and 40g) at a fixed pH value. In their findings, the particles sizes obtained for the 10 g honey were ranging from 18.98 nm to 26.05 nm and from the range of 15.63 nm to 17.86 nm for 40 g of honey which is four-fold of the former. Therefore, it can be concluded that honey concentrations do have an effect on the particle size of silver nanoparticles generated.

In the case of SBH concentrations lower than 25 mg/ml, there was no SPR peak observed. Thus, this is an evidence that no nanoparticles were formed at low SBH concentrations. The

highest absorbance peak is observed at SBH concentration of 100 mg/mL. Nevertheless, the peak does not have a uniform and smooth distribution. Therefore, the SBH concentration of 50 mg/mL was selected as the optimal honey concentration for the synthesis of AgNPs in this study because it gave an acceptable uniform smooth absorbance peak.

4.2.4 Effect of AgNO₃ concentration

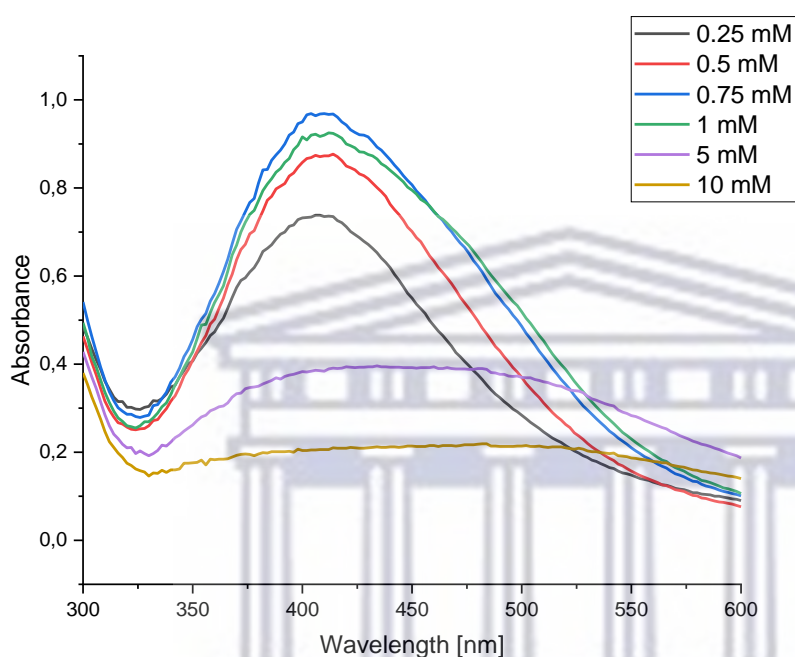


Figure 13: UV-Vis spectra of AgNPs at 75 °C, pH 10 and 50 mg/mL Honey concentration at different AgNO₃ concentration.

Upon investigating the effect of AgNO₃ concentration on the synthesis of SBH-AgNPs, it was observed that higher concentrations of AgNO₃ led to a decrease in recorded absorbance (See Figure 13). The 0.25 mM, 0.5 mM, 0.75 mM, 1 mM, 5 mM, and 10 mM AgNPs had a peak at 406 nm, 414 nm, 404 nm, 412 nm, 420 nm, and 434nm with absorbances of 0.738, 0.877, 0.969, 0.925, 0.364, and 0.212 respectively. The results obtained in this study are contradictory to those reported by Behravan and colleagues where they found that increasing the concentration of silver nitrate also increased the absorption peak. They concluded that increasing the AgNO₃ concentration led to more Ag⁺ being converted to Ag thereby increasing the amount of silver nanoparticles (Behravan et al., 2019). However, in their study they synthesized silver nanoparticles using a plant extract which is different from the reducing agent used in this study. In other literatures utilizing honey as the reducing agent, they did not investigate the effect of silver nitrate concentration and thus does not report it.

The change in amount of AgNO_3 brought variations in the observed SPR band of the SBH-AgNPs. Furthermore, as expected the SPR band was shifted to shorter or longer wavelengths with a change in AgNO_3 concentration. It was found that at higher concentrations of AgNO_3 at 5 mM and 10 mM the absorbance peak was significantly reduced and had a very broad distribution as well as a red shifted wavelength. The latter was similarly observed by Htwe, et al (2019) where they synthesized silver nanoparticles by green method but with varied concentrations of AgNO_3 . The absorption of silver nanoparticles at 0.5 mM showed a peak at 417 nm which then shifted to 424 nm at 0.7 mM, as was observed by HRSEM micrograph, that indeed the particles were increasing in size. The solution containing 0.75 mM AgNO_3 was used for subsequent synthetic purposes in that study (Htwe, et al., 2019).

4.3 Characterization of AgNPs

4.3.1 UV-vis spectroscopy analysis of the AgNPs

UV-vis spectroscopy is an analytical tool used to monitor the formation of silver nanoparticles. In metal nanoparticles such as in silver, the conduction band and valence band lie very close to each other in which electron moves freely. These free electrons give rise to a SPR absorption band (Taleb et al., 1998). It has been previously reported that the plasmon resonance peaks and line widths are sensitive to the shape and size of nanoparticles (Abou El-Nour et al., 2010). Hence, the existence of SPR peak is the primary signature of metal nanoparticle formation (Das et al., 2010), (Haiza, et al., 2013). The results obtained from the UV-vis absorption spectra of silver nanoparticles is shown in Figure 14. It gave a uniformly distributed absorption peak with a maximum wavelength of 414 nm.

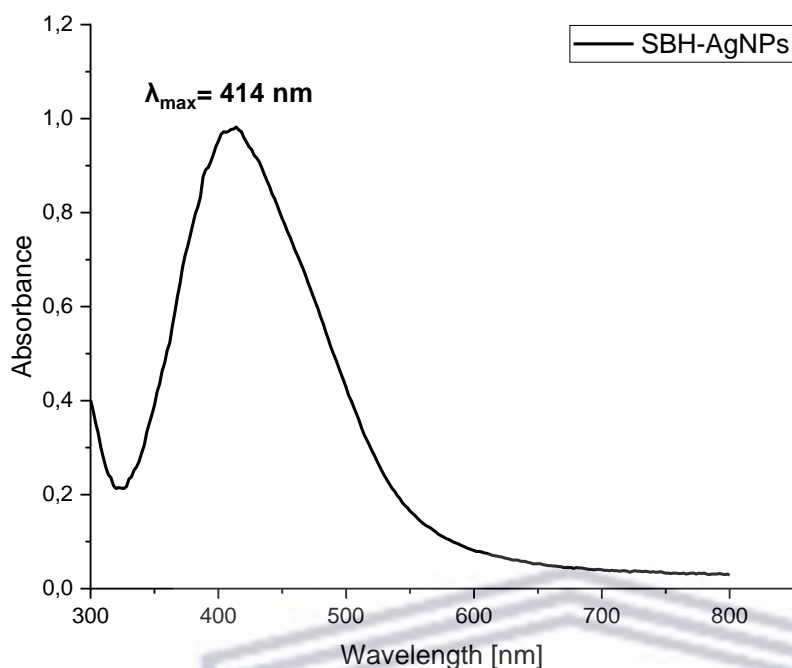


Figure 14: UV-vis spectra of SBH-AgNPs as synthesized at 75 °C, pH 10, 50 mg/mL Honey concentration and 0.75 mM of AgNO₃.

These results are in good agreement with previous evaluations done by Philip (2010). They synthesized AgNPs and obtained the SPR peak in the UV-vis spectra appearing at 413 nm (Philip, 2010). In a different study, Khorrami and colleagues synthesized silver nanoparticles and the SPR peak was visible at 426 nm (Khorrami et al., 2019). The SPR peak obtained from the UV-vis results on the study by Philip, (2010) is almost the same as the one obtained in this study (414 nm) and they also observed a smooth and narrow absorption band. The reaction of the silver nanoparticles was carried out in a controlled pH synthesis and the SPR they reported was found at a basic pH of 8.5. Similarly, in this study the smooth and uniformly distributed SPR band was observed in a basic pH of 10. It was previously reported that increasing the pH results in the greater wavelength of the absorbance peak which is the plausible explanation of the higher wavelength in our study (Fan, et al., 2015). However, in the study by Khorrami et al, (2019) they did not report the synthesis pH which makes it appear controversial.

4.3.2 FTIR analysis of the SBH and SBH-AgNPs

The FTIR measurements were carried out to identify the functional groups responsible for reducing capping and efficient stabilization of the AgNPs synthesized using stingless bee honey and AgNO₃. The comparison of the FTIR spectrum results of SBH sample, 50 mg/ml and SBH-AgNPs, synthesized using the optimal conditions, are displayed in Figure 15 below.

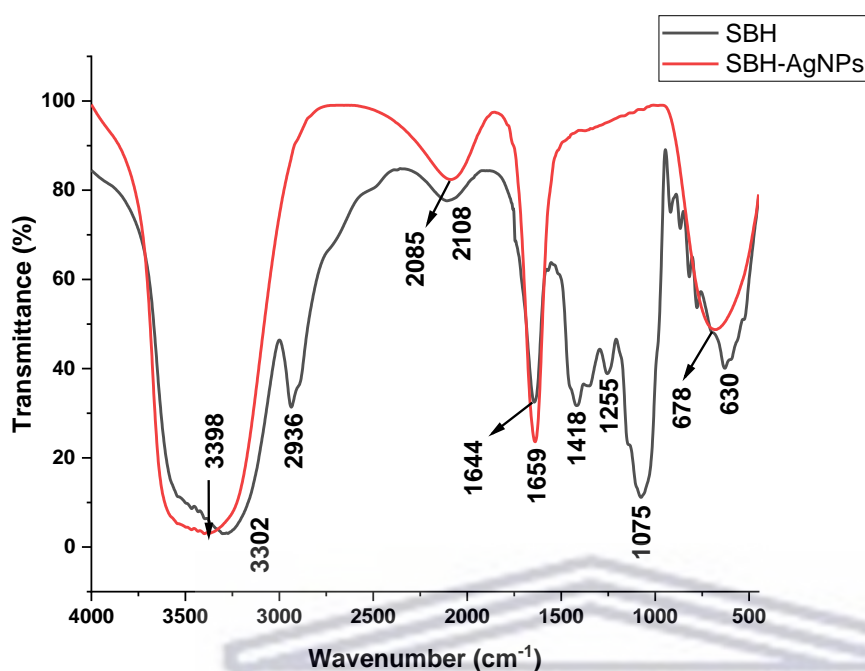


Figure 15: FTIR spectra of stingless bee honey and SBH-AgNPs.

According to Khorrami et al. (2019) honey has been found to contain a significant number of phenolic compounds, reducing sugars, proteins and vitamins. Based on the FTIR spectrum depicted in Figure 15, in the stingless bee honey spectrum appears a broad at 3302 cm^{-1} related to functional groups of phenols' OH. This peak is attributed to phenolic compounds found in the honey and this peak was also found in a study by Khorrami et al. (2019) when they were analysing the functional groups present in *Astragalus gossypinus* honey. A minor peak appeared in 2936 cm^{-1} is assigned to the CH groups of aldehydes. Aldehydes were among the compounds found in honey from *Melipona subnitida* and *M. scutellaris* by Costa et al. (2018) when they analysed honey samples using headspace-solid phase microextraction (HS-SPME) and gas chromatography coupled with mass spectrometry.

At around 1660 and 1535 cm^{-1} the amide I and II bands of proteins are expected to occur as prominent bands. In the present work, the band appears at 1644 cm^{-1} (Haiza, et al., 2013), (Khorrami et al., 2019). According to Kędzierska-Matysek et al. (2018) the vibration bands at around 1418 and 1347 cm^{-1} are characteristic for bending vibration of O-CH and C-CH in the carbohydrate structure which were also observed at 1418 cm^{-1} in this study. Another band appearing at 1255 cm^{-1} was observed which is comparable to a band around 1250 cm^{-1} that was also reported by Kędzierska-Matysek et al. (2018) is characteristic of the stretching vibration of C-H of the C-H in carbohydrates.

The strong peaks at 1075, and 630 cm^{-1} correspond to C-O and C=C stretching vibrations indicating the presence of vinyl ether and alkene compounds (Ghramh et al., 2020). The IR band present at 2108 cm^{-1} can possibly be characteristic of carbonyl group C=O stretching (Youssef et al., 2019). According to an investigation reported by Youssef et al (2019) they synthesized silver nanoparticles using honey and used FTIR to identify the functional groups present in honey responsible for the reduction of silver nitrate. They also observed a band at 2119 cm^{-1} which was characteristic of carbonyl group C=O stretching. The broad band found at around 3300- 3400 cm^{-1} arising from –OH stretching vibrations has been previously reported to be responsible for the presence of polyphenols on the honey. The –OH functional groups are the main components of phenols and flavonoids of the honey, and they play a major role in the formation of AgNPs (Hasim et al., 2020). Evidently, honey has been also reported to have some protein content in its composition and to confirm this, there is a band at 1644 cm^{-1} which has been indicated to be attributed to the presence of amides (proteins) (Hasim et al., 2020).

On the other hand, the FTIR spectrum of the SBH-AgNPs as shown in Figure 15 produced only 4 bands, at 3398, 2085, 2885, 1659, and 678 cm^{-1} indicating the presence of stabilizing and capping agent with the NPs. Some of the bands are similar to that obtained in the SBH spectrum while some peaks disappeared such as the band at 2936, 1418 and 1075 cm^{-1} . The broad band that appeared at 3398 cm^{-1} is assigned to the presence of the O-H stretch of alcohols. In a different study, Hasim et al. (2020) synthesized silver nanoparticles using Tualang honey. The FTIR spectra of the silver nanoparticles had a broad peak found at 3335 cm^{-1} attributed to (OH) vibrations of phenols (Hasim et al., 2020). Another peak observed at 2085 cm^{-1} may correspond to nitrile C \equiv N stretch or alkynyl C \equiv C stretch (Ghramh et al., 2020). While the peaks at 1659 and 678 cm^{-1} were assigned to the NH group of amines (Khorrami et al., 2019) and C=C stretching vibrations (Ghramh et al., 2020) respectively. Some peaks disappeared such as that corresponding to, CH functional groups of alkanes, and the CO group of carboxylic acids, respectively which could indicate that those functional groups were involved in the reduction and stabilization process of SBH-AgNPs. The existence of these identified functional groups then validated the successful reduction of AgNO₃ into biogenic AgNPs using honey.

The FTIR analysis confirms the idea that proteins (Hasim et al., 2020), polyphenols, amine groups (Khorrami et al., 2019), flavonoids, and other compounds reduce AgNO₃ to generate AgNPs. The molecules attached to the AgNPs appear to have free and bound amide groups, and these substances may be polyphenols with aromatic rings and bound amide regions, according to the IR spectra. Differences between the honey and AgNPs together with some

variance in the peak shift positions strongly suggest that the honey is what gives the AgNPs their stability.

4.3.3 HR-TEM analysis of AgNPs

The size and shape of nanoparticles synthesized using honey solution were measured using TEM instrumentation. To analyse the size distribution of SBH-AgNPs, ImageJ software was employed. EDS was also used to identify the elemental composition of the synthesized nanoparticles and an SAED pattern was obtained to analyse the crystallinity of the AgNPs. Figure 16 (A) shows a TEM micrograph of AgNPs synthesized using 50mg/mL of stingless bee honey solution.

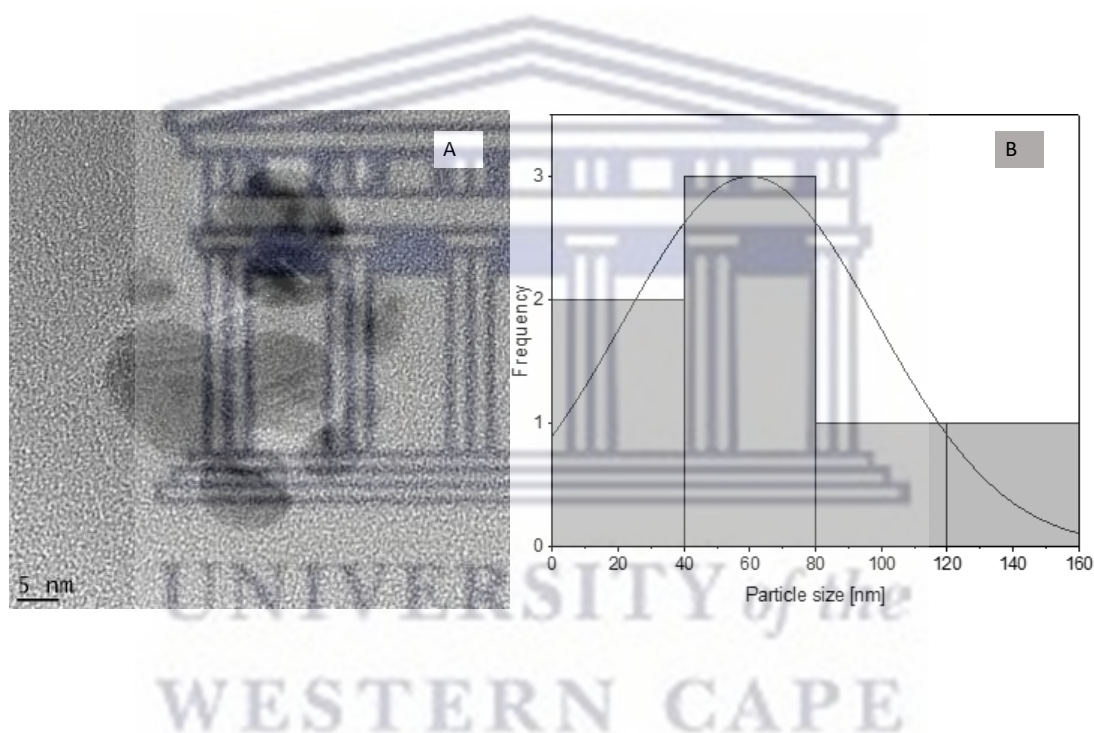


Figure 16: (A) HR-TEM image of SBH-AgNPs at 5 nm scale and (B) size distribution curve of the obtained SBH-AgNPs.

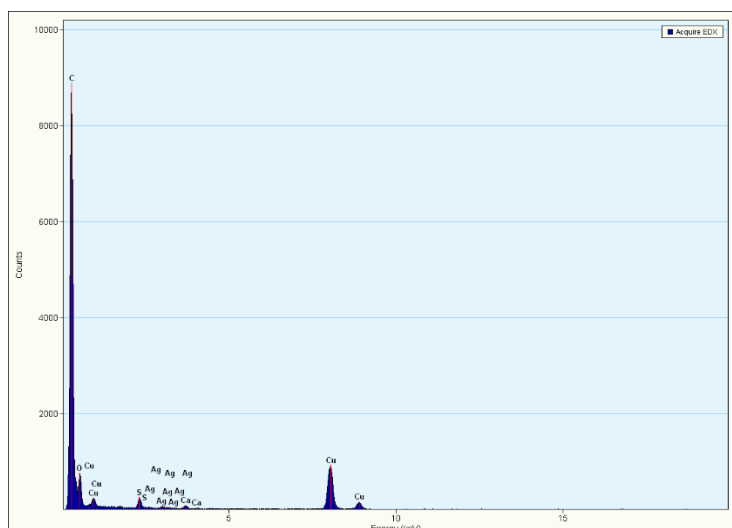


Figure 17: EDX characterization spectrum obtained for SBH-AgNPs. Visible peaks confirm the presence of silver, carbon and copper substances in the tested sample.

TEM image clearly shows the dispersion of silver nanoparticles supported (dark spherical particles) over honey matrix. The histogram indicated in Figure 16 (B) evaluated from the corresponding TEM image to determine average size of nanoparticles which was computed as 60 nm with broad size distribution. The TEM image showing the particles at 5 nm microscopic viewing shows darker spots and the particles appear to be agglomerating as there are some spherical nanoparticles joined together. The average size indicated by the TEM results is smaller than that obtained from the DLS analysis (79,67 nm) which was as expected. This is because the DLS measures the hydrodynamic size of the nanoparticles which encompasses the organic layer while TEM only measures the inorganic core size (Mourdikoudis et al., 2018). Coleman et al, (2011) compared several characterization techniques used to obtain data on particle size distributions. In their findings, DLS gave higher values than TEM. For instance, it gave 42 nm for a given silica reference sample which was reported to be 25 nm by TEM (Coleman et al., 2011). The quantitative analysis using EDX as depicted in Figure 17 showed relatively low silver content which confirms the presence of AgNPs. The spectrum also showed the presence of carbon and copper which results from the carbon-copper grid used for the analysis of the sample (Rodríguez-León et al., 2013), (Alsammarraie et al., 2018).

4.3.4 DLS analysis of AgNPs

A DLS analysis was used to measure size distribution, zeta potential and PDI values of the SBH-AgNPs as shown in Table 4. A particle size distribution's level of non-uniformity is referred to as "polydispersity." (Dos Santos, et al., 2012). The molecular weight distribution width is measured by the PDI, ranges from 0 to 1. Monodispersed nanoparticles are those with

a PDI value of less than 0.2. The broadening of the particle size distribution is shown by an increase in the PDI value (Bhattacharjee, 2016). The SBH-AgNPs have a PDI value of 0.36 and a hydrodynamic size about 79.67nm hence it can be concluded that these nanoparticles are polydispersed.

Table 4: Average size, PDI and zeta potential of the SBH-AgNPs synthesized using 50 mg/mL concentration of honey solution at 75 °C for 3 h.

Average size (nm)	PDI	Zeta potential (mV)
79.67	0.36	-15

Previous studies have described that the parameter that affects the characteristics of the silver nanoparticles is the PDI, which is largely influenced by the AgNO₃ concentration. Since monodisperse samples are more stable and have uniform morphologies, PDI values less than 0.3 are indicative of a monodisperse sample, which is strongly related to the zeta potential. In this sense, the reaction parameters' effects are uniform across all the examined characteristics. The size distribution, agglomeration, and shape of the resulting nanoparticles are all directly influenced by the reaction conditions used to synthesize Ag-NPs, which leads one to the conclusion that these results are very significant (Manosalva et al., 2019). The zeta potential of the SBH-AgNPs was determined and it was -15 mV. The negative charge suggests there are repulsive forces between the nanoparticles. In a different study, silver nanoparticles were synthesized using a leaf extract as a reducing agent (Anandalakshmi, et al., 2016). The DLS results indicated a broad spectrum of particle size distribution which had a value of 73.14 nm. Subsequently, the zeta potential of the AgNPs was reported to be -7.66 mV. It was suggested that the negative zeta potential indicates that the nanoparticles were stable, and their results agree with ours.

According to previous literature, it is indicated that metal nanoparticles that have a large negative zeta potential repel each other, hence they do not aggregate. Nevertheless, those with low zeta potential values can easily aggregate since there are no strong repulsive forces keeping them apart. Nanoparticles with negative or positive zeta potential values between ±10 to 20 mV are regarded as relatively stable (Ardani et al., 2017). A similar zeta potential value of 15.3 mV was reported by Jemilugba et al (2019) where they synthesized AgNPs using *Combretum erythrophyllum* plant leaves and they suggested that the mono-dispersity seen in their TEM

image indicates that the NPs have an appropriate surface charge for electrostatic stability to prevent aggregation. However, the latter is not true in our study as the TEM images show some degree of aggregation and thus it can be possibly that the honey is not a good stabilizing agent unlike in the case of plant extracts.

4.4 Antibacterial activity of AgNPs

4.4.1 Stability of SBH-AgNPs in biological media

Regarding AgNPs and other silver species, some of their interactions with culture media and their components have been reported by several authors. When culture media interact with AgNPs, they may affect their properties in different ways, such as the silver ion release rate, aggregation, or surface oxidation process (Vazquez-Muñoz, et al., 2020). The dispersion of nanosilver in a biological medium causes the surface-coating agents to re-establish equilibrium by mostly losing some of the coating molecules. When these coating agents are displaced by other molecules such as inorganic ions or water present in the media, the nanoparticles may no longer be stable therefore undergo aggregation. Additionally, in the presence of molecular oxygen, silver atoms can interact with molecular oxygen and become oxidized to silver ions (McShan, et al., 2014). The stability of SBH-AgNPs was evaluated in LB and MHB biological media over a 24h period as shown in Figure 18. These incubation temperatures are the most used for biological assays.

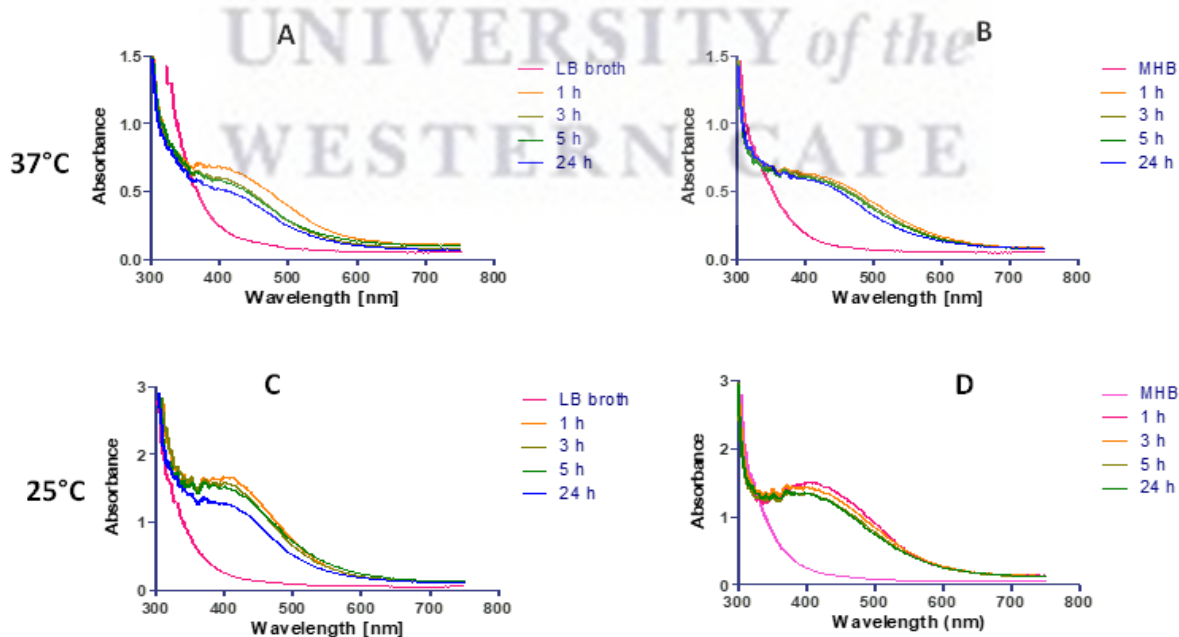


Figure 18: The UV-Vis spectra of SBH-AgNPs, recorded over a 24 h period (at 25 and 37 °C) after mixing with different biological media; MHB and LB broth.

Upon the addition of SBH-AgNPs to the LB broth and MHB, the UV-Vis absorption spectra did slightly change as shown in Figure 18 (A-D). The stability of SBH-AgNPs was measured at 37°C and 25 °C to observe the effect of the biological assay conditions towards their stability. It was noted that in the LB broth, there was a significant decrease in the absorbance spectra for both temperatures, hence it could be concluded that the SBH-AgNPs are stable in the MHB media. Therefore, using LB broth in the biological evaluation assays was discontinued. According to some authors, the pH of the media affects the stability of AgNPs. The silver ion release rate may be favoured in alkaline environments, which leads to faster degradation of the AgNPs. Therefore, the AgNPs are more stable in the MHB than the LB broth since the pH in LB broth is more alkaline than MHB. A recent study by Vazquez-Muñoz et al. (2020) evaluated the effects of the physicochemical properties of the culture medium on AgNP stability and antibacterial activity. It was found that the SPR peak of AgNPs in an acidic pH (6.2) was similar to the profile of AgNPs in the control solution (pH 7.2). However, AgNPs in the basic pH (8.2) solution had shown a different SPR peak. There was also an increase in the peak wideness which suggested an increasing oxidation of the AgNPs (Vazquez-Muñoz, et al., 2020).

4.4.2 Agar well diffusion assay

Antimicrobial results obtained from this study are shown in Table 5. An inhibition zone with diameter greater than 10 mm is considered as positive antagonism effect (Kumar & Kumar, 2015). The synthesized AgNPs show positive antagonism effect against almost all the selected bacterial strains except for MRSA which has a zone of inhibition that is not greater than 10 mm. The low inhibitory activity against MRSA can be expected since this bacterial strain has been reported to have high antibacterial resistance (Davies & Davies, 2010). The highest zone of inhibition of 13mm was measured against *S. epidermidis* and *P. aeruginosa* followed by 12 mm towards *S. aureus*, *K. pneumoniae* and *E. coli*. Meanwhile at 50 mg/mL concentration, the SBH did not show any inhibition for all the selected bacterial strains. This can be due to the fact that the honey solution has a very low concentration for it to show its antibacterial activity that is reported to be present in previous studies. In a study by Rosli and colleagues, they investigated the antibacterial activity of honey samples from eight stingless bees. The antibacterial studies indicated good antagonism effect against *S. aureus* at 50% concentration for all honey samples. At 12.5% concentration, only three honey samples showed inhibitory effect against one or more bacteria at the range of 10 to 16 mm in diameter of the inhibition zone. Thus, it can be suggested that the concentration of honey do have an effect its antibacterial activity (Rosli et al., 2020).

Additionally, in a different study, Temary et al, (2007) also investigated the antibacterial activity of honey sample from stingless bees. In their finding, the stingless bee honey did possess antibacterial activity against *Staphylococcus aureus*, *Enterococcus faecalis*, *Escherichia coli* and *Pseudomonas aeruginosa*. Agar well diffusion test showed that the honey inhibited the growth of bacteria at a concentration of 50 % (w/v) which is equivalent to 500 (mg/mL) (Temaru, et al., 2007). However, this concentration is higher than that tested in this study (50 mg/mL) which also suggests that the honey used in this study was very diluted which may have decreased its antibacterial activity. Since the optimal honey concentration that was selected during the optimization process was 50 mg/mL it was quantitatively correct to also use it for testing the antibacterial activity that it possesses at that particular concentration hence it was not increased to enhance its activity.

Table 5: The antibacterial effects of green synthesized SBH-AgNPs with the concentration of 63 µg/mL against six human pathogenic bacterial strains. (-) indicates no zone of inhibition.

Microorganisms	Zones of inhibition (mm)		
	SBH	SBH-AgNPs	Ciprofloxacin
<i>S. aureus</i>	-	12	22
<i>S. epidermidis</i>	-	13	27
MRSA	-	10	21
<i>K. pneumoniae</i>	-	12	28
<i>E. coli</i>	-	12	34
<i>P. aeruginosa</i>	-	13	24

The obtained antibacterial findings of AgNPs are comparable with those obtained by Jemilugba et al (2019) where they synthesized AgNPs with an average size of 13.62 nm using plant leaves as a reducing agent. The zone of inhibition for their AgNPs against *S. aureus*, *E. coli* and *S. epidermidis* were found to be 15, 12 and 12 mm respectively (Jemilugba et al., 2019). Although they had synthesized smaller nanoparticles compared to the ones in our study with an average size of 60 nm, it is interesting to note that they showed similar antibacterial activity against those mentioned bacterial strains. In another study they reported a green synthesis of AgNPs

using honey and evaluated their antibacterial activity. To their findings, the AgNPs showed increasing susceptibility in the order of *S. aureus* < *K. pneumoniae* < *P. aeruginosa* < *E. coli* with zone of inhibition diameter of 20.00, 23.33, 25.00 and 29.33 mm respectively (Youssef et al., 2019). According to the reported literature on the antibacterial activity of silver nanoparticles using green synthesis, they did not report the concentration of the AgNPs, but they do assess the antibacterial activity of silver nanoparticles against some of the bacterial strains which are selected in this study. Khorrami et al, (2019) reported the antibacterial activity of silver nanoparticles synthesized using *Astragalus gossypinus* honey from plants.

Agar diffusion assay was used to study the antibacterial activity of AgNPs and the honey against *S. aureus*, *P. aeruginosa* and *E. coli*. The activity of AgNPs was evaluated using different concentrations of 64, 125, 250, 500 and 100 µg/mL. The results revealed that the AgNPs at the concentration of 64 µg/mL, there was no activity against all the three tested strains. However, at AgNPs concentrations of 125 µg/mL some degree of inhibition was found but against only *S. aureus*, and it was 10 mm. In the other concentrations, AgNPs had significant antibacterial activity against all the three bacterial strains. The activity of these nanoparticles was found to be concentration dependent (Khorrami et al., 2019). According to the concentration of 64 µg/mL of the *Astragalus gossypinus* honey synthesized AgNPs, the activity of SBH-AgNPs in our study appears to be more significant.

4.4.3 MIC and MBC of AgNPs

The MIC is reported as the lowest Ag-NP concentration which inhibits bacterial growth and MBC as the Ag-NP concentration in which no bacterial growth occurs. The MIC and MBC of SBH-AgNPs was investigated against six pathogens, namely *S. aureus*, *S. epidermidis*, MRSA, *P. aeruginosa*, *E. coli* and *K. pneumoniae* as indicated in Table 6. The SBH-AgNPs showed activity against all the microorganisms tested. In contrast, the honey solution did not display significant activity against all the selected strains. However, SBH-AgNPs were mostly active against *S. epidermidis*, with MIC and MBC values of 16 and 32 µg/mL, respectively. The lowest antibacterial activity recorded for SBH-AgNPs was against MRSA, with MIC and MBC values of 63 and 125 µg/mL, respectively. SBH-AgNPs exhibited the same inhibitory activity against *S. aureus*, *E. coli* and *P. aeruginosa*, with an MIC and MBC value of 63 µg/mL. Similarly, the zone of inhibition recorded against MRSA microorganism, the MBC was higher than all the other bacterial strains due to the resistant nature of this human bacteria. Contrastingly, Youssef et al (2019) reported better inhibitory activity with MIC values

against, *P. aeruginosa*, *E. coli* and *K. pneumoniae* of 6.3, 6.3 and 12.5 µg/mL respectively. As revealed by the results shown in Table 5, there is no definite MIC value trend for both Gram-negative and Gram-positive bacteria. In the case of Gram-negative organisms, the silver nanoparticles must pass through the thin peptidoglycan layer and outer membrane. Gram-positive bacteria lack the outer membrane and have a thick (30 nm) peptidoglycan layer (Feng et al., 2000), (Slavin et al., 2017). Therefore, the physical barrier that the particles must pass does not vary significantly. In a different study, Khorrami and colleagues reported the MIC and MBC of their honey synthesized silver nanoparticles. It was discovered that this nanoparticle's MIC and MBC against *S. aureus* were 100 g/mL and 200 g/mL, respectively. In contrast better efficacy of the AgNPs was observed against Gram-negative microorganisms *P. aeruginosa* and *E. coli* at lower doses of 24.5 g/mL for both the MIC and MBC.

Table 6: The Minimum inhibitory assay and minimum bactericidal assay (µg/mL) of SBH-AgNPs and honey solution against the most common pathogens. (-) indicates no antibacterial activity.

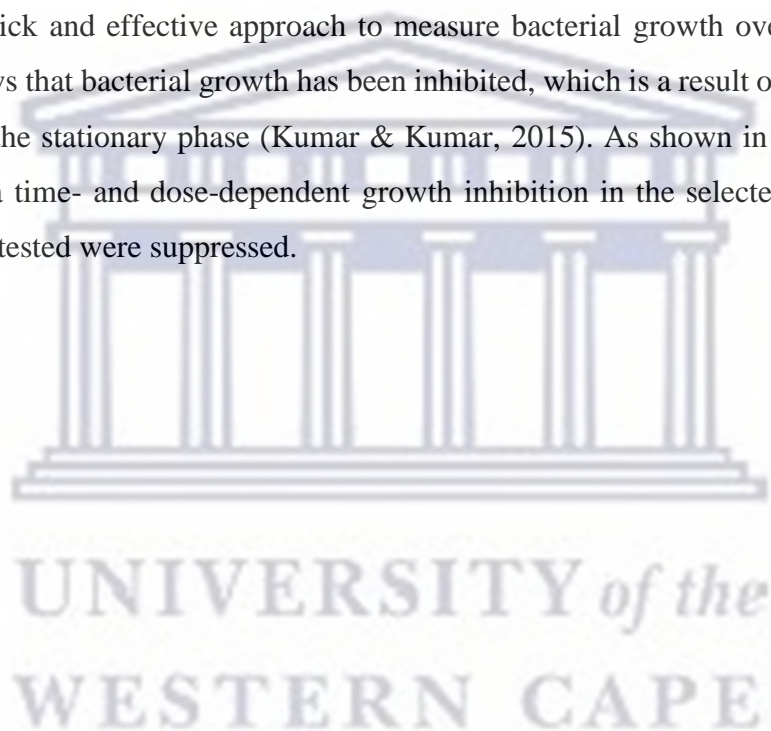
Microorganisms	SBH		AgNPs		Ciprofloxacin	
	MIC	MBC	MIC	MBC	MIC	MBC
<i>S. aureus</i>	-	-	63	63	0.5	1
<i>S. epidermidis</i>	-	-	16	32	0.25	0.25
MRSA	-	-	63	125	0.5	2
<i>K. pneumoniae</i>	-	-	32	32	0.02	1
<i>E. coli</i>	-	-	63	63	0.02	1
<i>P. aeruginosa</i>	-	-	63	63	0.5	2

In most cases, Ag-NPs' bactericidal activity is brought on by their adhesion to bacterial cell walls. As a result, this attachment generates an accumulation of envelope protein precursor, which in turn results in protein denaturation, proton motivation force reduction, and ultimately cell death (Yu-sen et al., n.d.). The size of the NPs has a significant impact on the bactericidal activity they exert against pathogens. Smaller NPs are more readily absorbed by the bacterial cell membranes. This is because smaller particles have higher surface area for interacting with

microbes and releasing Ag^+ through oxidation. These speeds up the production of reactive oxidant species, which further compromises cellular structure and ultimately leads to cell death (Chudasama et al., 2010). In our study the nanoparticles had a larger average size of 60 nm which may have caused them to be slightly slower to be absorbed or penetrate the bacterial cell membrane.

4.4.4 Growth inhibitory kinetics of SBH-AgNPs

The bacterial growth kinetics of six bacterial strains was evaluated in response to treatment with the SBH-AgNPs. Figure 19 show the effects of SBH -AgNPs on the bacterial growth of six bacterial strains. Bacterial growth was evaluated using variations in optical density (OD). This offers a quick and effective approach to measure bacterial growth over time. Reduced absorbance shows that bacterial growth has been inhibited, which is a result of cell death being blocked during the stationary phase (Kumar & Kumar, 2015). As shown in Figure 19, SBH-AgNPs caused a time- and dose-dependent growth inhibition in the selected strains. All six bacterial strains tested were suppressed.



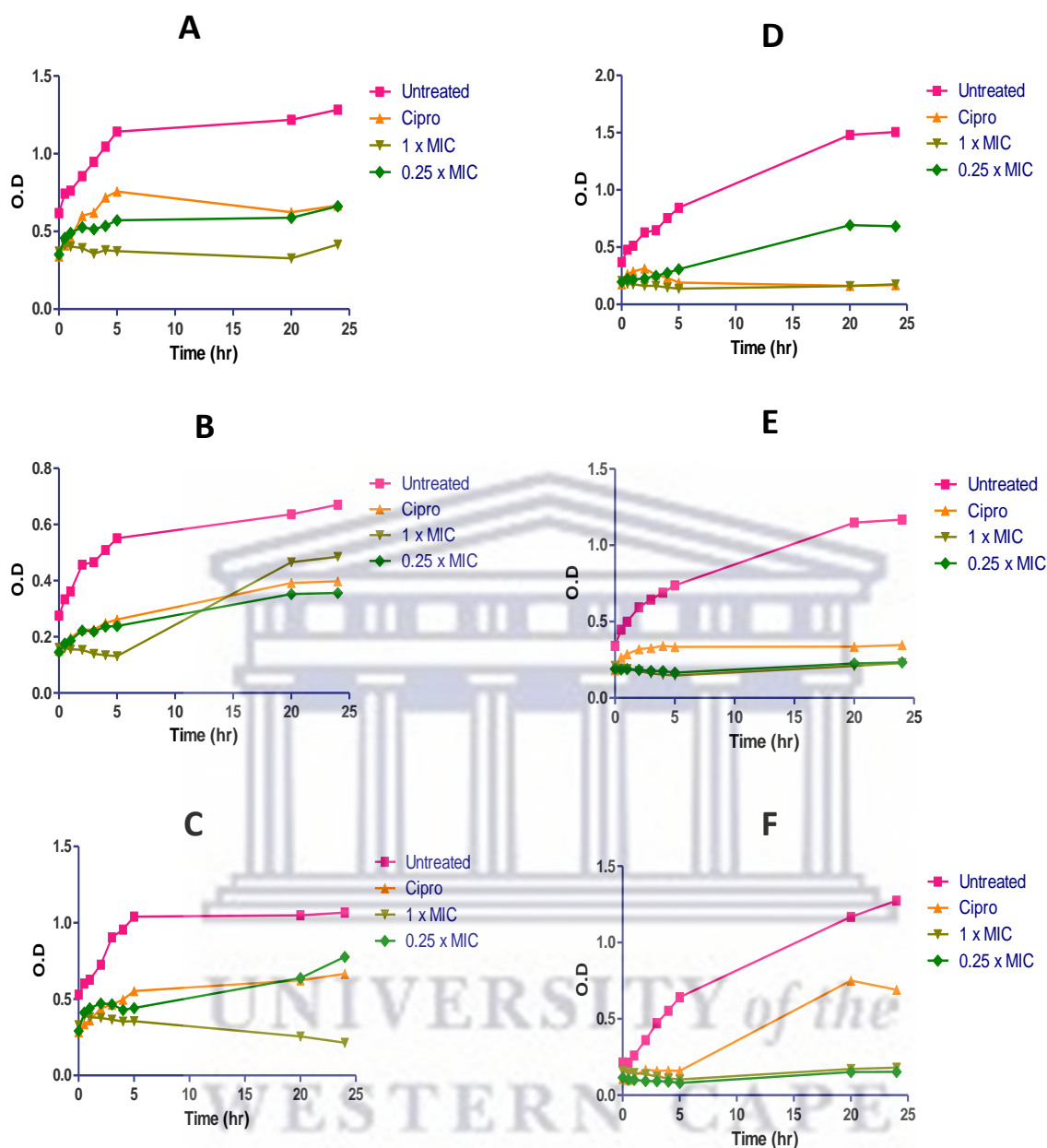


Figure 19: Growth inhibitory activity of AgNPs at 1X MIC (250 $\mu\text{g}/\text{mL}$) and 0.25X MIC (63 $\mu\text{g}/\text{mL}$) against selected Gram-positive and Gram-negative bacteria. (A) represents *S. aureus*, (B) *S. epidermidis*, (C) MRSA, (D) *K. pneumoniae*, (E) *E. coli* and (F) *P. aeruginosa*. The positive control ciprofloxacin was used at a concentration of 2 $\mu\text{g}/\text{mL}$.

The growth curve of *S. aureus* shows good inhibitory activity of the SBH-AgNPs for both MIC concentrations and interestingly both these curves are below the positive control (ciprofloxacin) from 0 to 24 hours. However, a varying trend is observed in the growth curve of *S. epidermidis* as the inhibitory effect at MIC of 250 $\mu\text{g}/\text{mL}$ drastically diminish after 5 hours. A similar observation on the growth curve of MRSA occurred and the bactericidal effects of SBH-AgNPs at 63 $\mu\text{g}/\text{mL}$ showed a decline in inhibitory effect after 5 hours. The

growth curves of (D) *K. pneumoniae*, (E) *E. coli* and (F) *P. aeruginosa* show that SBH-AgNPs are able to effectively inhibit the growth of these three organisms from 0 to 24 hours at MIC concentration of 250 µg/mL. Contrastingly, the growth curve on gram positive bacteria, *S. epidermidis* does not show any growth inhibitory effect at MIC concentration of 250 µg/mL after 5 hours while the other positive strains do display a growth decline. Overall, the SBH-AgNPs showed improved inhibitory effect against gram-negative bacteria than in gram-positive bacteria. The explanation behind this observation could be because Gram-negative bacteria lack the thick peptidoglycan layer found in Gram-positive bacteria, which may potentially act as a protective layer, the cell wall breakdown that results from physical interaction between NPs and the cell wall is more harmful for Gram-negative bacteria (Slavin et al., 2017).

This study, however, is subject to several limitations. The instrumentation used for analysing SBH-AgNPs was limited due to time constraints and unavailability of certain instruments. XRD analysis was not performed to study the crystallinity of the silver nanoparticles. It is possible that the stingless bee honey possess significant anti-inflammatory properties as stated in the previous literature hence exploring this anti-inflammatory characteristic could be beneficial to this research study. Lastly, there is limited research on the *Meliponula feriguenaea* stingless bee honey composition and its properties.



UNIVERSITY of the
WESTERN CAPE

References

- Ghaffari-Moghaddam, M. and Hadi-Dabanlou, R., 2014. Plant mediated green synthesis and antibacterial activity of silver nanoparticles using *Crataegus douglasii* fruit extract. *Journal of Industrial and Engineering Chemistry*, 20(2), pp.739-744.
- Yuqing, M., Jianrong, C. and Keming, F., 2005. New technology for the detection of pH. *Journal of biochemical and biophysical methods*, 63(1), pp.1-9.
- Behravan, M., Panahi, A.H., Naghizadeh, A., Ziaee, M., Mahdavi, R. and Mirzapour, A., 2019. Facile green synthesis of silver nanoparticles using *Berberis vulgaris* leaf and root aqueous extract and its antibacterial activity. *International journal of biological macromolecules*, 124, pp.148-154.
- da Costa, A.C.V., Sousa, J.M.B., Bezerra, T.K.A., da Silva, F.L.H., Pastore, G.M., da Silva, M.A.A.P. and Madruga, M.S., 2018. Volatile profile of monofloral honeys produced in Brazilian semiarid region by stingless bees and key volatile compounds. *LWT*, 94, pp.198-207.
- Khorrami, S., Jafari Najafabadi, F., Zarepour, A. and Zarrabi, A., 2019. Is *Astragalus gossypinus* honey a natural antibacterial and cytotoxic agent? An investigation on *A. gossypinus* honey biological activity and its green synthesized silver nanoparticles. *BioNanoScience*, 9, pp.603-610.
- Kędzierska-Matysek, M., Matwijczuk, A., Florek, M., Barłowska, J., Wolanciuk, A., Matwijczuk, A., Chruściel, E., Walkowiak, R., Karcz, D. and Gładyszewska, B., 2018. Application of FTIR spectroscopy for analysis of the quality of honey. In *BIO Web of Conferences* (Vol. 10, p. 02008). EDP Sciences.
- Haiza, H., Azizan, A., Mohidin, A.H. and Halin, D.S.C., 2013. Green synthesis of silver nanoparticles using local honey. In *Nano Hybrids* (Vol. 4, pp. 87-98). Trans Tech Publications Ltd.
- Htwe, Y.Z.N., Chow, W.S., Suda, Y. and Mariatti, M., 2019. Effect of silver nitrate concentration on the production of silver nanoparticles by green method. *Materials Today: Proceedings*, 17, pp.568-573.
- Taleb, A., Petit, C. and Pileni, M.P., 1998. Optical properties of self-assembled 2D and 3D superlattices of silver nanoparticles. *The Journal of Physical Chemistry B*, 102(12), pp.2214-2220.

Abou El-Nour, K.M., Eftaiha, A.A., Al-Warthan, A. and Ammar, R.A., 2010. Synthesis and applications of silver nanoparticles. *Arabian journal of chemistry*, 3(3), pp.135-140.

Das, R., Nath, S.S., Chakdar, D., Gope, G. and Bhattacharjee, R., 2010. Synthesis of silver nanoparticles and their optical properties. *Journal of Experimental Nanoscience*, 5(4), pp.357-362.

Philip, D., 2010. Honey mediated green synthesis of silver nanoparticles. *Spectrochimica Acta Part A: Molecular and Biomolecular Spectroscopy*, 75(3), pp.1078-1081.

Ghramh, H.A., Ibrahim, E.H. and Kilany, M., 2020. Study of anticancer, antimicrobial, immunomodulatory, and silver nanoparticles production by Sidr honey from three different sources. *Food science & nutrition*, 8(1), pp.445-455.

Youssef, G.A., El-Boraey, A.M. and Abdel-Tawab, M.M., 2019. Eco-friendly green synthesis of silver nanoparticles from egyptian honey: Evaluating its antibacterial activities. *Egyptian Journal of Botany*, 59(3), pp.709-721.

Hasim, H., Rao, P.V., Sekhar, A.C., Muthuraju, S., Asari, M.A. and Sirajudeen, K.N.S., 2020. Green synthesis and characterization of silver nanoparticles using Tualang honey and evaluation of their antioxidant activities. *Advances in Natural Sciences: Nanoscience and Nanotechnology*, 11(2), p.025010.

Mourdikoudis, S., Pallares, R.M. and Thanh, N.T., 2018. Characterization techniques for nanoparticles: comparison and complementarity upon studying nanoparticle properties. *Nanoscale*, 10(27), pp.12871-12934.

Coleman, V.A., Jämting, Å.K., Catchpoole, H.J., Roy, M. and Herrmann, J., 2011, September. Nanoparticles and metrology: a comparison of methods for the determination of particle size distributions. In *Instrumentation, Metrology, and Standards for Nanomanufacturing, Optics, and Semiconductors V* (Vol. 8105, pp. 13-19). SPIE.

Rodríguez-León, E., Iñiguez-Palomares, R., Navarro, R.E., Herrera-Urbina, R., Tánori, J., Iñiguez-Palomares, C. and Maldonado, A., 2013. Synthesis of silver nanoparticles using reducing agents obtained from natural sources (*Rumex hymenosepalus* extracts). *Nanoscale research letters*, 8, pp.1-9.

Alsammarraie, F.K., Wang, W., Zhou, P., Mustapha, A. and Lin, M., 2018. Green synthesis of silver nanoparticles using turmeric extracts and investigation of their antibacterial activities. *Colloids and Surfaces B: Biointerfaces*, 171, pp.398-405.

Radwan, R., Abdelkader, A., Fathi, H.A., Elsabahy, M., Fetih, G. and El-Badry, M., 2021. Development and evaluation of letrozole-loaded hyaluronic acid/chitosan-coated poly (d, l-lactide-co-glycolide) nanoparticles. *Journal of Pharmaceutical Innovation*, pp.1-12.

Dos Santos, K.C., da Silva, M.F.G., Pereira-Filho, E.R., Fernandes, J.B., Polikarpov, I. and Forim, M.R., 2012. Polymeric nanoparticles loaded with the 3, 5, 3'-triiodothyroacetic acid (Triac), a thyroid hormone: factorial design, characterization, and release kinetics. *Nanotechnology, science and applications*, pp.37-48.

Bhattacharjee, S., 2016. DLS and zeta potential—what they are and what they are not?. *Journal of controlled release*, 235, pp.337-351.

Manosalva, N., Tortella, G., Cristina Diez, M., Schalchli, H., Seabra, A.B., Durán, N. and Rubilar, O., 2019. Green synthesis of silver nanoparticles: effect of synthesis reaction parameters on antimicrobial activity. *World Journal of Microbiology and Biotechnology*, 35, pp.1-9.

Anandalakshmi, K., Venugobal, J. and Ramasamy, V.J.A.N., 2016. Characterization of silver nanoparticles by green synthesis method using *Petalium murex* leaf extract and their antibacterial activity. *Applied nanoscience*, 6, pp.399-408.

Ardani, H.K., Imawan, C., Handayani, W., Djuhana, D., Harmoko, A. and Fauzia, V., 2017, April. Enhancement of the stability of silver nanoparticles synthesized using aqueous extract of *Diospyros discolor* Willd. leaves using polyvinyl alcohol. In *IOP Conference Series: Materials Science and Engineering* (Vol. 188, No. 1, p. 012056). IOP Publishing.

Jemilugba, O.T., Parani, S., Mavumengwana, V. and Oluwafemi, O.S., 2019. Green synthesis of silver nanoparticles using *Combretum erythrophyllum* leaves and its antibacterial activities. *Colloid and Interface Science Communications*, 31, p.100191.

Vazquez-Muñoz, R., Bogdanchikova, N. and Huerta-Saquero, A., 2020. Beyond the nanomaterials approach: Influence of culture conditions on the stability and antimicrobial activity of silver nanoparticles. *ACS omega*, 5(44), pp.28441-28451.

McShan, D., Ray, P.C. and Yu, H., 2014. Molecular toxicity mechanism of nanosilver. *Journal of food and drug analysis*, 22(1), pp.116-127.

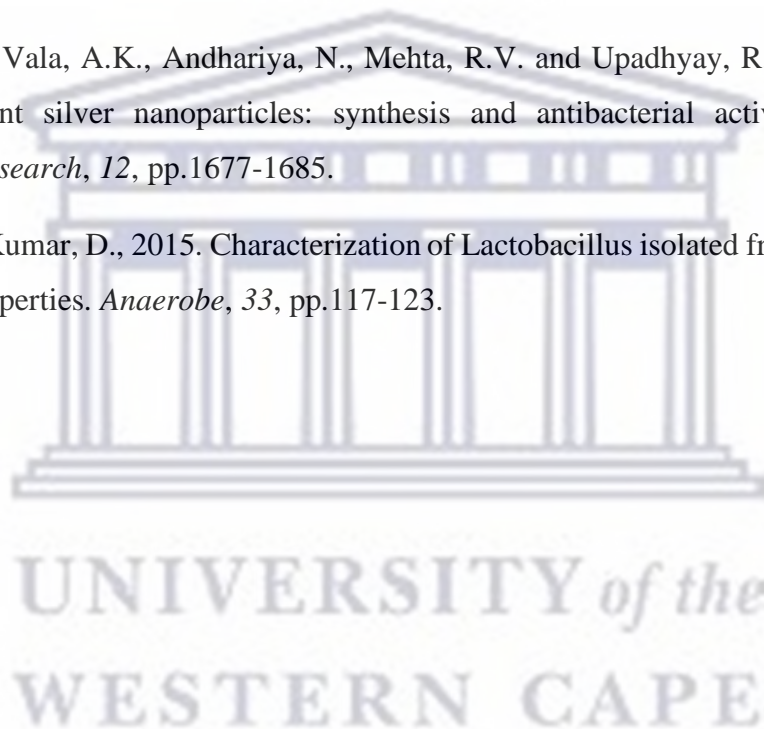
Davies, J. and Davies, D., 2010. Origins and evolution of antibiotic resistance. *Microbiology and molecular biology reviews*, 74(3), pp.417-433.

Rosli, F.N., Hazemi, M.H.F., Akbar, M.A., Basir, S., Kassim, H. and Bunawan, H., 2020. Stingless bee honey: Evaluating its antibacterial activity and bacterial diversity. *Insects*, 11(8), p.500.

Yu-sen, E.L., Vidic, R.D., Stout, J.E., McCartney, C.A. and Victor, L.Y., 1998. Inactivation of *Mycobacterium avium* by copper and silver ions. *Water research*, 32(7), pp.1997-2000.

Chudasama, B., Vala, A.K., Andhariya, N., Mehta, R.V. and Upadhyay, R.V., 2010. Highly bacterial resistant silver nanoparticles: synthesis and antibacterial activities. *Journal of Nanoparticle Research*, 12, pp.1677-1685.

Kumar, A. and Kumar, D., 2015. Characterization of *Lactobacillus* isolated from dairy samples for probiotic properties. *Anaerobe*, 33, pp.117-123.



Chapter 5

Conclusions and recommendations

5.1 Conclusions

AgNPs were successfully synthesized using stingless bee honey, characterized, and evaluated for antibacterial activity for the very first time according to the best of our knowledge, the study's aims and objectives were met.

The optimum conditions for the synthesis of SBH-AgNPs were honey solution of 50 mg/mL (pH 10) at temperature of 75°C and AgNO₃ concentration of 0.75 mM over a period of 3 hours under dark. The SBH-AgNPs had an SPR peak at 414 nm after synthesis. The DLS analysis showed that the hydrodynamic size was 79.67 nm with a PDI of 0.36 and the zeta potential had a value of -15 mV which indicated moderate stability.

HR-TEM results confirmed that the SBH-AgNPs are spherical in shape with an average core diameter of 60 nm with a broad size distribution. FTIR analysis confirms that proteins, polyphenols, amine groups, flavonoids, and other compounds present in the honey were able to reduce AgNO₃ to generate AgNPs. The FTIR spectra obtained revealed similarities between the extracts and AgNPs along with some variation in peak shift positions, which sufficiently confirms the idea that phytochemicals are responsible for the reduction. The EDX confirms that there are Ag elements present in the sample.

After successful determination of the physiochemical properties of the SBH-AgNPs, biological studies were performed to assess their antibacterial activity. The antibacterial studies showed that the SBH-AgNPs do exhibit antibacterial effects. Agar well diffusion was carried out and SBH-AgNPs showed some degree of potency against the different bacterial strains within this study. The highest zone of inhibition of 13 mm was displayed against both *S. epidermidis* and *P. aeruginosa*. However, there was no inhibition zone visible for the stingless bee honey in all the tested strains. The MIC and MBC assays indicated that SBH-AgNPs were mostly active against *S. epidermidis*, with MIC and MBC values of 16 and 32 µg/mL, respectively. Although, it had been previously reported that agar well diffusion is not a reliable antibacterial activity test, but it was carried out in this study as the primary method for determining antibacterial susceptibility and it also aids in visualization of growth inhibition. The lowest activity recorded for SBH-AgNPs was against MRSA, with MIC and MBC values of 63 and 125 µg/mL,

respectively. Lastly, growth kinetics revealed that the SBH-AgNPs did inhibit the growth of the selected bacteria strains even at lower concentrations. However, against *S. epidermidis* at SBH-AgNPs concentrations equal to the MIC (250 µg/mL) there was no growth inhibition observed.

5.2 Recommendations

1. We highly recommend a further examination of the antibacterial activity of the stingless bee honey by using the concentrations higher than 50 mg/mL.
2. Secondly, the stability and the broad size distribution of SBH-AgNPs can be improved by introducing a capping or stabilizing agent such as Chitosan because it is biocompatible polysaccharide with positive Z potential which can stabilize negative charged nanoparticles.
3. It is very important to identify the compounds in the SBH and analyse those which are responsible for the capping of AgNPs.
4. It has been reported that stingless bees honey possess anti-inflammatory properties, therefore in the future, the anti-inflammatory tests need to be carried out.

5.3 Future work

To develop a method to stabilize the AgNPs produced. In order to acquire antimicrobial activity for the SBH alone, a higher concentration of stingless bee honey of more than 50 mg/ml can potentially be used in the agar well diffusion assay. Additionally, anti-inflammatory studies for the stingless bee honey can also be conducted.

To use HPLC on the analysis of honey and SBH-AgNPs for identifying the phytochemicals which are responsible for antimicrobial activity. Furthermore, these phytochemicals can be isolated and used for antimicrobial applications.

Studying the mechanism of interaction of SBH-AgNPs with biological systems to be able to develop nanoparticles with favourable physiochemical properties which will not produce negative effects.